



HAL
open science

Fractional degassing of S, Cl and F from basalt magma in the Bárðarbunga rift zone, Iceland

Olgeir Sigmarsson, Séverine Moune, Pierre-J Gauthier

► **To cite this version:**

Olgeir Sigmarsson, Séverine Moune, Pierre-J Gauthier. Fractional degassing of S, Cl and F from basalt magma in the Bárðarbunga rift zone, Iceland. *Bulletin of Volcanology*, 2020, 82 (7), 10.1007/s00445-020-01391-7. hal-03001649

HAL Id: hal-03001649

<https://uca.hal.science/hal-03001649>

Submitted on 19 Nov 2020

HAL is a multi-disciplinary open access archive for the deposit and dissemination of scientific research documents, whether they are published or not. The documents may come from teaching and research institutions in France or abroad, or from public or private research centers.

L'archive ouverte pluridisciplinaire **HAL**, est destinée au dépôt et à la diffusion de documents scientifiques de niveau recherche, publiés ou non, émanant des établissements d'enseignement et de recherche français ou étrangers, des laboratoires publics ou privés.

Copyright

Fractional degassing of S, Cl and F from basalt magma in the Bárðarbunga rift zone, Iceland

Olgeir Sigmarsson^{1,2}, Séverine Moune^{1,3}, Pierre-Jean Gauthier¹

¹Laboratoire Magmas et Volcans, Université Clermont Auvergne - CNRS, Campus Universitaire des Cézeaux, 6 avenue Blaise Pascal, 63178 Aubière, France

²NordVulk, Institute of Earth Sciences, University of Iceland, 101 Reykjavik, Iceland

³Observatoire Volcanologique et Sismologique de Guadeloupe, Institut de Physique du Globe de Paris, France
(e-mail: olgeir.sigmarsson@uca.fr)

Accepted in Bulletin of Volcanology

Key words: Rayleigh distillation, volcanic gas, partition coefficients, Holuhraun lava, Kilauea, Etna

Abstract

The composition of gas emitted from a volcano producing basalt magma can vary during an eruption and according to the volcano-tectonic setting of the degassing vents. Post-eruptive filter-pack gas samples from the 2014-2015 Holuhraun crater in the Bárðarbunga rift zone have lower ratios of S over halogens (Cl and F) and elevated F/Cl (~50 times lower S/Cl and ~5 times higher F/Cl; mass ratios) compared to samples of the syn-eruptive gas plume. The compositional changes are readily explained by Rayleigh distillation with decreasing sulphur concentrations and increasing concentrations of halogens and F relative to Cl in the final gas phase. For Cl the vapour-melt partition coefficient ($\mathcal{D}^{V/M}$) decreased from 13-85 to 2.2 during residual degassing, whereas that of F remained uniform at approximately 1.8. Distinctly different degassing behaviour is observed for Cl and F. High \mathcal{D} for Cl may indicate an important influence of sulphur and water on Cl volatility in basaltic melt, whereas that of F remains unaffected. The primary gas of the Holuhraun magma had similar ratios of S over Cl and F as observed at the Kilauea rift zone which, together with lower S/halogens in the residual gas in both cases, suggests similar degassing mechanism. By inference, initial CO₂ degassing is likely to have occurred subglacially close to the Bárðarbunga central volcano before and during the 2014-2015 eruption on the rift-related fissure swarm.

Introduction

Degassing of basaltic magma is known to impact the environment by emission of several different gaseous species but the physics of the degassing process is less well understood. At depth, where CO₂ is the dominant volatile species, gas segregation from basaltic or low-viscosity magma is thought to follow a cyclic behaviour, which may lead to alternating explosive and effusive activity (Sparks, 2003). The gas phase and the rising melt can evolve from a state of thermodynamic equilibrium to that of a progressive open-system fractional distillation, especially during the waning stage of an eruption (Aiuppa, 2009). Fractional degassing at shallow depth has been inferred from changing gas composition during single eruptions from craters at different altitude and during different types of volcanic activity, as in the case of the persistently degassing Mount Etna, Sicily (e.g. Aiuppa et al., 2002; Burton et

51 al., 2003; Allard et al., 2005). In addition, the syn-eruptive gas phase of a basaltic fissure
52 eruption is expected to be different from the residual gas phase of a cooling lava during
53 emplacement and crystallization (Swanson & Fabbi, 1973). A well-known example of a
54 basaltic fissure eruption is that of Laki in Iceland which may have released up to 20% of the
55 total emitted SO₂ and significant proportion of the halogens during lava field emplacement
56 and crystallisation (Thordarson et al., 1996). The final degassing stage may thus lead to local
57 hazes with different gas composition than the principal gas phase. Fluorine, for instance, with
58 its relatively high solubility in basaltic melt compared to Cl and S (Carroll & Webster, 1994),
59 will principally enter the final gas phase. Such degassing of F can lead to fluorosis in grazing
60 animals, a well-known effect that caused the death of approximately two thirds of the
61 Icelandic livestock during and soon after the Laki eruption (Thorarinsson, 1969; Pétursson et
62 al., 1984; Thordarson and Self, 2003).

63
64 Variations in the gas composition at basaltic volcanoes are also related to the global tectonic
65 context, with hotspot volcanoes generally emitting gas of higher S/halogens than those in
66 subduction-zone settings, despite several common factors as reviewed by Aiuppa (2009). At
67 Kilauea, Hawaii, gas of different composition is released at summit craters than is emitted in
68 flank eruptions in rift zones (e.g. gas type I and II of Gerlach & Graeber, 1985; Greenland et
69 al., 1988; Symonds et al., 1994; Edmonds et al., 2009). Likewise, during the 2001 eruption of
70 Etna, Burton et al. (2003) observed remarkably similar S/halogens in gas from the Northeast
71 crater (NEC) and the Central craters as well as in the bulk gas plume, whereas gas from the
72 Southeast crater (SEC) had considerably lower S/halogens and that of the flank crater, which
73 fed the 2001 summer lava flow, had even lower ratios. Their results confirmed observations
74 by Aiuppa et al. (2002), which in addition measured decreasing Cl/F in gas from the flank
75 crater. These studies suggest a primary gas phase from single magma body degassing beneath
76 NEC and Central craters, whereas SEC and the southern flank crater emitted a secondary gas
77 phase. Aiuppa (2009) extended the open system Rayleigh-type degassing model for Etna to
78 other basaltic volcanoes, a model that assumes uniform vapour-melt partition coefficients for
79 S, Cl and F. A similar method was applied by Mather et al. (2012) when discussing degassing
80 mechanism at Kilauea. However, neither Cl nor F volatility and their partition coefficients
81 between vapour and melt phases are well understood. A comparison of the primary gas phase
82 released during basaltic fissure eruption to that produced during the final degassing stages at
83 the end of an eruption should provide better constraints on the mechanism, volatile solubility,
84 and therefore the volatile partition coefficients between the silicate melt and the gas phase,
85 needed for better understanding of the degassing processes.

86
87 In this article syn- and post-eruptive gas phases of the Holuhraun eruption (29 August 2014 to
88 27 February 2015) within the rift zone of the Bárðarbunga volcanic system in Iceland are
89 compared. The eruption site was located approximately 40 km N of the Bárðarbunga central
90 caldera, which is positioned above the presumed centre of the Iceland mantle plume. The
91 eruptive fissure produced approximately 1.5 km³ of basalt of uniform composition (ol-tholeiite)
92 and liberated close to 10 Tg of SO₂ into the atmosphere (Sigmundsson et al., 2014; Gíslason et
93 al., 2015; Gauthier et al., 2016; Bali et al., 2018; Halldórsson et al., 2018; Pfeffer et al., 2018).
94 The large amount of gas emission from Holuhraun caused repeated air pollution events
95 characterized by atmospheric SO₂ concentrations exceeding air quality standards, as well as
96 high concentrations of fine-grained volcanogenic aerosols (Ilyinskaya et al., 2017; Stefánsson
97 et al., 2017). Snow precipitated around the lava field, rain and the surrounding rivers were
98 monitored during the eruption and had elevated F concentrations (Gíslason et al., 2015;
99 Galeczka et al., 2017; Stefánsson et al., 2017) despite its very low abundance in the main gas
100 plume (Gauthier et al., 2016). Understanding the origin and fate of fluorine during degassing

101 processes is thus of importance in order to assess its release to the atmosphere and subsequent
102 environmental impact. Here, results are presented on S and halogen (Cl and F) concentrations
103 in the post-eruptive gas phase released at Holuhraun in order to verify whether or not fluorine
104 is ultimately degassed and if a simple Rayleigh distillation process occurring during the
105 progressive basalt degassing explains the observed gas compositions. Halogen partition
106 coefficients $D^{\text{vapour/melt}}$ are estimated for Cl and F from S/Cl and S/F ratios and their variability
107 towards the end of the eruption is assessed. The results are finally compared with those from
108 Etna and Kilauea volcano (e.g., Gerlach & Graeber, 1985; Aiuppa et al., 2002; Burton et al.,
109 2003; Allard et al., 2005; Edmonds et al., 2009; Mather et al., 2012) and show that the gas phase
110 composition reflects the intrinsic parameters of the fractional degassing mechanism.

111 112 113 **Sample collection and analysis**

114 High-quality syn-eruptive gas samples are not easily collected during intense effusive activity
115 such as the Holuhraun eruption. Two syn-eruptive gas plume samples could be collected in still
116 weather on 2 October 2014, when the gas plume was grounded for a few hours because of a
117 short-lived temperature inversion of the atmosphere (Gauthier et al., 2016; Fig. 1). A few
118 months later, 21 January 2015, a third sample of the gas plume was collected from a helicopter
119 (Ilyinskaya et al., 2017). This latter sample has an order of magnitude lower SO₂ concentration
120 compared to the earlier samples, possibly reflecting greater air dilution on the plume's edge, or
121 increasing distance from the vent.

122
123 Recently published results (Stefánsson et al., 2017; Ilyinskaya et al., 2017) on ground-collected
124 syn-eruptive gas composition can be compared with those given by Gauthier et al. (2016). Out
125 of four filter-pack gas samples collected during the eruption by Stefánsson et al. (2017), three
126 have very similar S/Cl mass ratios with an averaged value of 41 ± 7 , characteristic of the syn-
127 eruptive gas plume (Gauthier et al., 2016). In marked contrast, their samples exhibit much
128 higher fluorine concentrations than reported by Gauthier et al. (2016), leading to lower Cl/F
129 ratios, somewhat intermediate between primary vapour compositions (Gauthier et al., 2016)
130 and residual vapour compositions (this work, Table 1). Marked enrichments in fluorine may
131 arise though from other sources than the syn-eruptive gas phase, such as secondary vapour from
132 the cooling lava field. The same holds true for ground-collected gas samples taken by Ilyinskaya
133 et al. (2017), who also suggested that extreme variability in their own samples may be explained
134 by a gas phase “partially sourced from the degassing lava”. In addition to the fortunate two
135 samples from Gauthier et al. (2016), we therefore consider only their helicopter-aided airborne
136 plume sample as representative of the principal syn-eruptive gas phase (Ilyinskaya et al., 2017).
137 Despite being strongly diluted compared to the gas plume samples of Gauthier et al. (2016), the
138 helicopter-aided sample from Ilyinskaya et al. (2017) has identical syn-eruptive S/Cl but
139 significantly lower S/F and Cl/F.

140
141 Ten days after the lava extrusion ended, the residual gas phase released from the cooling magma
142 was collected. Three post-eruptive filter-pack samples were obtained in calm weather on 9
143 March 2015 inside the main crater, approximately 50 m above the cooling lava lake (Fig. 1).
144 Intensive degassing was observed from the lava-filled crater with visually estimated maximum
145 gas emission from cracks inside the crater walls, one of which was selected for gas sampling.

146
147 The same filter-pack technique as presented in Gauthier et al. (2016) was employed. Each filter
148 pack was connected to a pump operating at a flow rate of 11 l/min for 23-72 min, collecting
149 three gas and aerosol samples (HH1, HH2 and HH3; Table 1) from a total air volume of 0.25-
150 0.79 m³. For comparison, the atmospheric composition free of volcanic gas (blank) was

151 collected approximately 500 m west of the lava field over one hour. Filters were subsequently
152 analysed for S, Cl and F concentrations using ion chromatography at ICCF-Sigma, Université
153 Clermont Auvergne, with analytical uncertainty of approximately 5%. For the consolidated and
154 thus outgassed lava, S concentration was measured with a CHNS/O analyser at LMV-
155 Université Clermont Auvergne, but those of Cl and F using absorption spectrophotometry and
156 selective electrodes, respectively, at CRPG-Nancy, France. The 2σ errors for S, Cl and F
157 concentrations in the lava are less than 10%.

158 159 **Results**

160 The post-eruptive gas phase has S, Cl and F concentrations two to three orders of magnitude
161 higher than the atmospheric background, which is therefore neglected. The gas samples are
162 characterised by S, Cl and F concentrations ranging from 49-164, 53-104 and 27-46 (in mg/m³),
163 respectively, and their composition significantly differs from the syn-eruptive gas plume. The
164 S concentrations in the post-eruptive gas phase are lower than those emitted during the primary
165 eruptive phase by a factor of 3 on average. In marked contrast, both Cl and F are in much higher
166 concentrations in the post-eruptive gas: 11 times more Cl and 62 times more F. The S/Cl mass
167 ratio is close to unity (0.92 - 1.58), substantially lower than the 40-52 of the primary gas phase
168 (Gauthier et al., 2016). So is the Cl/F mass ratio, which is on average 2 in the post-eruptive gas
169 phase against 11 ± 4 in the syn-eruptive plume. Consequently, the S/F mass ratio (1.85 - 3.53)
170 is two orders of magnitude lower in the final gas phase and its decline is already observed in
171 the late January 2015 gas (Table 1). Although S remains the principal minor gas component,
172 these observations suggest a much stronger halogen contribution to the vapour phase at the end
173 of the eruption.

174 175 176 **Discussion**

177 *Arguments for almost complete S degassing*

178 The sulphur-rich gas plume from the Holuhraun eruption affected people over most part of
179 Iceland because of the high volatility of S from the olivine tholeiitic basalt. Sulphur is known
180 to degas from basaltic melt until melt quenching or solidification, which for example explains
181 higher concentrations in water- vs air-quenched tephra, and tephra vs crystallized lava
182 (Thordarson et al., 1996; Óladóttir et al., 2007; Haddadi et al., 2017). The very low S
183 concentration in the degassed lava (97 ppm; Gauthier et al., 2016) compared to the initial
184 amount preserved in melt inclusions (up to 1644 ppm S; Bali et al., 2018) suggests that 94% of
185 sulphur was lost during magma ascent and evolution. Sulphide minerals could play a role in the
186 sulphur budget of the Holuhraun products since a few globules were observed in the early lava
187 and tephra in September 2014. However, most of the sulphides are present as irregular, partially
188 dissolved particles and exhibit variable S isotope composition, whereas other isotope ratios
189 remain mostly constant (Halldórsson et al., 2018). These sulphides are partially xenocrystic and
190 most likely picked up during magma ascent. Smaller euhedral sulphide spheres are crystallized
191 immiscible melt in the Holuhraun magma itself. However, they are scarce enough to ensure that
192 their crystallization (acting as a S sink) and their destabilization (acting as a S source) does not
193 drastically change the S budget at Holuhraun. It thus appears that most of the sulphur escaped
194 the magma as a volatile species before the crystallisation of the lava, mostly as gaseous SO₂
195 since H₂S does not exceed a few percent in the gas phase (Gíslason et al., 2015). With SO₂
196 averaging *ca* 30% in the gas phase (e.g. Bali et al., 2018), the S liquid-gas partition coefficient
197 ($D^{l/g}(S)$) can be estimated at $97 \cdot 10^{-6} / 0.15 = 6 \cdot 10^{-4}$. The figure must be considered as a maximum
198 value for $D^{l/g}(S)$ (note that $D^{l/g}$ is simply the reciprocal of $\mathcal{D}^{V/M}$) because the final S
199 concentration in the most degassed eruptive products could be lower than 97 ppm. Whichever
200 the exact value, it appears reasonable to assume $D^{l/g}(S)$ close to nil. Finally, even if some S

201 remains in quenched groundmass glass or in the rare sulphides, the bearing on its partition
202 coefficient between vapour and melt ($\mathcal{D}^{V/M}$) is none, since that coefficient only measures the
203 vapour-melt partition but neither vapour-glass nor melt-solid fractionation.

204

205 *Estimation of vapour/melt partition coefficients of Cl and F*

206 In contrast to S, which is severely depleted in the final solid product, Cl and F concentrations
207 in the crystallized lava reach 110 and 190 ppm, respectively, which is within the range observed
208 in melt inclusions and the lava groundmass (Gauthier et al., 2016; Bali et al., 2018). Moreover,
209 given their higher solubility in basaltic melt (Carroll & Webster, 1994), both Cl and F are
210 expected to degas principally at or very close to the surface. The important decreases in S/Cl,
211 S/F and Cl/F from the syn-eruptive gas plume to the post-eruptive gas phase clearly indicate
212 decreasing availability of S for the gas phase in the crystallizing basalt magma and increasing
213 relative concentrations of Cl and especially F in the final gas phase. This concentration pattern
214 strongly suggests a Rayleigh distillation process, with most of the S extracted from the melt.
215 The Rayleigh law, $C = C_0 \times f^{D-1}$, where C denotes the measured concentration of a given gas
216 species, C_0 its initial gas concentration, f the fraction of gas remaining in the magma (vapour
217 plus melt) and D the concentration in liquid divided by that of the gas (i.e. the partition
218 coefficient, $D^{l/g}$) can be linearized as:

219

$$220 \log Cl = \log Cl_0 + (D_{Cl}^{l/g} - 1) \times \log f$$

$$221 \log S = \log S_0 + (D_S^{l/g} - 1) \times \log f$$

222

223 When $D^{l/g}(S)$ is close to zero and can be neglected, the equations can be combined to eliminate
224 f, which leads to:

225

$$226 \log Cl = (1 - D_{Cl}^{l/g}) \times \log S - [(1 - D_{Cl}^{l/g}) \times \log S_0] + \log Cl_0.$$

227

228 The $D^{l/g}(Cl)$ can thus be determined from the slope of the linear relationship between log Cl
229 and log S. The vapour/melt partition coefficient ($\mathcal{D}^{V/M}$) for Cl, being simply the reciprocal of
230 $D^{l/g}(Cl)$, thus can readily be calculated. The $\mathcal{D}^{V/M}$ for F is obtained in the same way. Note that
231 if $D^{l/g}(S)$ were slightly higher than 0, these calculated $\mathcal{D}^{V/M}$ for halogens would be the maximum
232 possible values.

233

234 The results are plotted in Figure 2 where Cl and S concentrations in gas samples collected
235 during the eruption form a strong linear correlation ($R^2 = 0.990$). From the slope a surprisingly
236 low $D^{l/g}(Cl)$ is calculated that leads to unusually high value for $\mathcal{D}^{V/M}$ ($= 1/D^{l/g} = 85$), meaning
237 that 85 times more mass of Cl went into the gas phase compared to what remained in the melt
238 phase. The results from Stefánsson et al. (2017) fall on the lower concentration end of the
239 correlation. Taken together with the present results, a somewhat lower regression coefficient
240 ($R^2 = 0.987$) is obtained and a slope that yields less extreme $\mathcal{D}^{V/M}$ of 13. At first glance, our
241 values might seem extreme, but in fact, they are on the same order of magnitude as the highest
242 experimentally determined $\mathcal{D}^{V/M}$ by Stelling et al. (2008) and Alletti et al. (2009; $\mathcal{D}^{V/M}$ for Cl
243 as high as 24). Given the difficulties in determining $\mathcal{D}^{V/M}$ for Cl, such as the presence or absence
244 of a third phase (i.e. brine) in the experimental products (Webster et al., 1999), we consider the
245 value of 13 to 85 realistic, albeit possibly a maximum value. Chlorine most likely formed gas
246 species and outgassed at very low pressure, close to or at the surface, aided by extensive water
247 and sulphur degassing. In fact, evidence for sulphur-aided degassing of Cl does exist. Sulphur
248 chloride species such as S_2Cl can form in a gas phase, depending on the H/C and oxygen

249 fugacity (Zolotov & Matsui, 2002), and complex ligands such as $S_2Cl_2^{4-}$, S_2Cl^{3-} , SCl_2^{3-} , and
250 $S\cdot Cl_2^{3-}$ have been proposed for volatile transport of platinum-group elements (Fleet & Wu,
251 1993). Clearly experimental results are needed to improve understanding of sulphur degassing
252 effect on the volatility of Cl in mafic magma. The slope of the trend line for the three post-
253 eruptive gas samples ($R^2 = 0.84$) is significantly lower leading to an order of magnitude smaller
254 $\mathcal{D}^{V/M}$ for Cl, or only 2.2. The low $\mathcal{D}^{V/M}$ in the post-eruptive gas phase could reflect the decreased
255 role of a carrier gas for Cl such as H_2O or SO_2 , which concentrations can be assumed as
256 relatively low in the post-eruptive gas phase. Interestingly, similar $\mathcal{D}^{V/M}$ has been determined
257 in several experimental studies on Cl solubility in basalt without much sulphur present (Webster
258 et al., 1999; Stelling et al., 2008; Alletti et al., 2009). Such a low $\mathcal{D}^{V/M}$ for Cl may thus be
259 characteristic for residual degassing of basalts with a gas phase with relatively low S/Cl as
260 observed at Holuhraun.

261
262 Fluorine concentrations in all syn-eruptive samples show more scatter, possibly due to
263 contributions from different sources as suggested by Ilyinskaya et al. (2017). Therefore, we
264 again calculate best fit only for the two plume samples of Gauthier et al. (2016) and the
265 helicopter-aided sample of Ilyinskaya et al. (2017). The resulting $\mathcal{D}^{V/M}$ for F in the syn-eruptive
266 gas phase is close to that obtained for the three post-eruptive gas samples: 1.9 vs 1.7,
267 respectively. The much lower $\mathcal{D}^{V/M}$ for F compared to Cl during the eruption illustrates its
268 higher solubility in the basaltic melt, whereas in the residual gas phase similar volatility is
269 obtained for both halogens. Knowledge of $\mathcal{D}^{V/M}$ for F is limited and experimental results are
270 needed to test the accuracy of our approach. The halogen concentration in the residual gas phase
271 is thus approximately twice that of the final crystallizing melt.

272 273 *Comparison with Etnean gas*

274 Halogen degassing has been extensively studied at Mount Etna, where persistent open-conduit
275 degassing presents ample opportunities for gas sampling. Fractional degassing was proposed
276 for the 2000 eruption at the SE crater where variations of S/Cl correlated with eruptive
277 behaviour (Allard et al., 2005). Moreover, temporal decline of S/Cl and Cl/F was observed from
278 the central craters to the flank lava-forming eruption in 2001 (Aiuppa et al., 2002; Burton et al.,
279 2003). Despite the obvious difference between the subduction zone-related Etna stratovolcano,
280 where gas was sampled from several craters at different altitude, and Holuhraun in the
281 Bárðarbunga rift zone, where both syn- and post-eruptive gas was sampled from the same
282 fissure crater, an interestingly similar degassing patterns can be observed. In Figure 2, the S, Cl
283 and F gas concentrations from Aiuppa et al. (2002) are plotted and the slope of the best-fit lines
284 used to infer the vapour-melt partition coefficients for Cl and F during the 2001 flank eruption.
285 Severe S depletion relative to the halogens was observed and the calculated $\mathcal{D}^{V/M}$ for Cl is 2.3,
286 and 1.8 for F, indistinguishable from that of the Holuhraun post-eruption gas phase. Flank
287 eruptions at Etna thus bear similarities with fractional degassing at Holuhraun and, as suggested
288 by Aiuppa et al. (2002, 2009), with that of Kilauea volcano, Hawaii. However, Etna produces
289 gas especially enriched in Cl, as expected from its subduction-zone settings. The much higher
290 gaseous S concentrations and S/Cl at the hotspot-related Bárðarbunga and Kilauea is worth
291 further discussion.

292 293 *Comparison with Kilauea*

294 In Figure 3, we compare the S/Cl and S/F mass ratios measured in syn- and post-eruptive gas
295 phases of Holuhraun, as well as in the degassed lava. The decreasing trend observed from the
296 syn-eruptive gas plume through the residual gas phase to the degassed lava is consistent with a
297 simple Rayleigh fractionation. The simplest explanation for the observed behaviour is

298 progressive distillation of S from the rift-zone magma. When the eruption ceases, lava cools
299 down and residual volatiles form a gas phase causing the melt to crystallise. The flux of carrier
300 gas (mostly H₂O and SO₂) is still important enough to flush halogens out of the cooling lava
301 but the low S concentration in the residual melt leads to a drastic decrease in Cl volatility, and/or
302 increase in Cl solubility. Because fraction f of volatiles remaining in the melt decreases as the
303 outgassing progresses, the Rayleigh equation implies increasing halogens, and notably fluorine,
304 concentrations, not only in gas collected close to the degassing lava but also in the near-
305 environment. The volcanic haze of basaltic fissure eruptions consequently comprises, in
306 addition to water and sulphur dioxide, chlorine and fluorine gas species that may carry many
307 metal and metalloid species out of the final melt of crystallizing basaltic lava. Accordingly,
308 plume samples collected close to advancing lava field, like those sampled by Stefánsson et al.
309 (2017) and Ilyinskaya et al. (2017) are prone to be mixed with F-enriched vapour, as
310 exemplified in Figure 3 where their samples lie in between the two end members.

311
312 Gauthier et al. (2016), and more recently Edmonds et al. (2018), showed that hotspot-related
313 volcanoes exhibit common trace-element degassing patterns. One of the best-studied hotspot
314 basaltic volcanoes is Kilauea, Hawaii. Although the geodynamics of Bárðarbunga volcano is
315 under the influence of both the Iceland mantle plume and extensional tectonics, while Kilauea
316 is merely related to the Hawaii hotspot, their volcano-tectonic context is surprisingly
317 comparable. Type II SO₂-rich gas is characteristic of the Kilauea east rift zone (Gerlach and
318 Graeber, 1985), and also of the gas plume released from the Holuhraun craters in the
319 Bárðarbunga fissure swarm (= rift zone). In addition, both volcanoes share common physical
320 parameters such as a magma velocity of ~1 m.s⁻¹ (Swanson et al., 1979; Eaton et al., 1987;
321 Parfitt & Wilson, 1994; Gauthier et al., 2016). Therefore, the comparison of S/Cl and S/F mass
322 ratios at both volcanoes is relevant for better understanding degassing processes at basaltic
323 volcanoes. It can be seen in Figure 3 that syn-eruptive gas samples from the rift zone of Kilauea
324 and the Bárðarbunga fissure swarm (Holuhraun) have similar S/Cl and S/F ratios. The same
325 holds true for residual gases as well as the most degassed products collected at Kilauea. In fact,
326 a continuous trend of decreasing S concentrations is observed from Type II gas of the Kilauea
327 rift zone (Symonds et al., 1994) towards the Pele's tears of one of the rift-zone craters (Edmonds
328 et al., 2009). Gas burst and lava spatter data extend this trend to even lower S/halogens. The
329 simplest explanation is a progressive distillation of S from the rift-zone magma leading to
330 decreasing solubility and increasing volatility of the halogens.

331
332 Within this framework, it might seem surprising not to detect at Bárðarbunga-Holuhraun the
333 equivalent of CO₂-enriched Type I gas released from the Halema'uma'u crater inside the
334 Kilauea caldera (Gerlach and Graeber, 1985). Indeed, the gas from Kilauea's summit crater
335 exhibits the highest recorded S/Cl and S/F ratios (Mather et al., 2012) and it likely represents
336 the very first step of the Rayleigh distillation process (Figure 3). Whether such primary gas is
337 absent or hidden within the Bárðarbunga volcanic system is worth considering. Gauthier et al.
338 (2016) observed that ²¹⁰Po, a short-lived isotope from the highly volatile element polonium,
339 was at unusually low level in the main gas plume released from the Holuhraun craters. Their
340 preferred interpretation was that earlier degassing of Po, and of CO₂ which was also depleted
341 in the main gas plume, took place somewhere under the glacier-covered Bárðarbunga caldera
342 and the magma pathway towards the Holuhraun fissure craters. Because of the ice cover of
343 Bárðarbunga, such a first-stage CO₂-enriched gas phase remains obscure and hard to detect.
344 Nevertheless, ice-cauldrons formed 1-5 km SE of Bárðarbunga during the rifting event in the
345 second-half of August 2014 (Reynolds et al., 2019), and shortly before the eruption started,
346 could be the surface manifestations of CO₂-rich gas burst during magma ascent. Alternatively,
347 the chimney of seismicity detected 12 km SE of Bárðarbunga caldera and interpreted to be

348 caused by vertical melt migration from 24 km depth towards the brittle-ductile crustal transition
349 at 9 km could be another candidate for the site of early CO₂ degassing (Hudson et al., 2017).

350

351 **Conclusion**

352

353 The different compositions of the syn- and post-eruptive gas emitted during the Holuhraun
354 2014-2015 eruption is explained by fractional degassing following the Rayleigh distillation law.
355 Since S is extremely volatile, its partition into the gas phase can be assumed close to
356 quantitative. In that case, the vapour-melt partition coefficient $\mathcal{D}^{V/M}$ can be calculated for both
357 Cl and F from their correlation with S concentrations. Elevated $\mathcal{D}^{V/M}$ for Cl during the eruption
358 may reflect the effect of sulphur degassing on Cl concentration, but experimental verification
359 is needed to test this proposition. In the post-eruptive gas phase, $\mathcal{D}^{V/M}(\text{Cl})$ is significantly lower,
360 most likely because S is strongly depleted at the end of the Rayleigh process, and Cl and F reach
361 similar vapour-melt partition coefficients. Improved knowledge of $\mathcal{D}^{V/M}$ for minor volatile
362 species is required for the use of halogens in gas monitoring at active basaltic volcanoes (e.g.,
363 Aiuppa, 2009) but our study suggests a complex behaviour, partly dependent on sulphur
364 degassing. Further constraints on $\mathcal{D}^{V/M}(\text{Cl})$ will also aid interpretation of Cl isotopes, which are
365 known to fractionate during degassing (Sharp et al., 2010).

366

367 An open-system Rayleigh-type outgassing of the lava field explains elevated F concentrations
368 measured in the environmental samples close to the lava field. Sustained halogen, and notably
369 fluorine, degassing from cooling lavas may play a major role in the transportation of volatile
370 trace elements. The results of this study underline the importance of integrating post-eruptive
371 degassing processes when quantifying the entire volcanic gas emissions and their impact on the
372 environment.

373

374 The mass ratios of sulphur over halogens (S/Cl and S/F) in the gas phase illustrate a strong
375 analogy between degassing processes operating at both Kilauea and Bárðarbunga volcanoes. In
376 contrast to Kilauea, CO₂-enriched primary gases were not released into the atmosphere during
377 the Holuhraun eruption. However, we speculate that the ice cauldrons generated before and
378 during lateral magma transfer beneath the Vatnajökull ice-sheet resulted from CO₂ gas burst
379 rather than small sub-glacial eruptions.

380

381

382 **Acknowledgment**

383 The field mission was financed by the French Laboratory of Excellence Program “ClerVolc”
384 and Institute of Earth Science, University of Iceland through Icelandic Governmental Civil
385 Protection Grant. Sveinbjörn Steinþórsson and Ármann Höskuldsson are acknowledged for
386 field assistance and photos taken during the gas sampling. Magnús T. Guðmundsson and
387 Guðmundur H. Guðfinnsson are thanked for discussion on ice-cauldron formations and
388 correcting the English. Comments from two anonymous reviewers were appreciated as well as
389 the editorial handling by the three editors: Patrick Allard, Tobias Fischer and Jacopo Taddeucci.
390 This is ClerVolc contribution number 411.

391

392

393 **References**

394 Aiuppa A, Federico C, Paonita A, Pecoraino G, Valenza M (2002) S, Cl and F degassing as
395 an indicator of volcanic dynamics: The 2001 eruption of Mount Etna. *Geophys Res Lett* 29:
396 1556. doi:10.1029/2002GL015032.

397

398 Aiuppa A (2009) Degassing of halogens from basaltic volcanism: insights from volcanic gas
399 observations. *Chem Geol* 263: 99–109.
400

401 Allard P, Burton M, Muré F (2005) Spectroscopic evidence for a lava fountain driven by
402 previously accumulated magmatic gas. *Nature* 433: 407–410.
403

404 Alletti M, Baker DR, Scaillet B, Aiuppa A, Moretti R, Ottolini L (2009) Chlorine partitioning
405 between a basaltic melt and H₂O–CO₂ fluids at Mount Etna. *Chem Geol* 263: 37–50.
406

407 Bali E, Hartley ME, Halldórsson SA, Guðfinsson GH, Jakobsson S (2018) Melt inclusion
408 constraints on volatile systematics and degassing history of the 2014–2015 Holuhraun
409 eruption, Iceland. *Contrib Mineral Petrol* 173: 9.
410

411 Burton M, Allard P, Muré F, Oppenheimer C (2003) FTIR remote sensing of fractional
412 magma degassing at Mount Etna. In: Oppenheimer C, Pyle D, Barclay J (eds.), *Volcanic
413 degassing*. Geological Society, London, Special Publication 2213: 281–293.
414

415 Carroll MR, Webster JD (1994) Solubilities of sulfur, noble gases, nitrogen, chlorine,
416 and fluorine in magmas. In: Carroll MR, Holloway JR (eds.) *Volatiles in Magmas*. *Rev
417 Mineral Geochem* 30: 231–279.
418

419 Eaton JP, Richter DH, Krivoy HL (1987) Cycling magma between the summit reservoir and
420 Kilauea Iki lava lake during the 1959 eruption of Kilauea volcano. *US Geol Surv Prof Pap*
421 1350: 1307–1335
422

423 Edmonds M, Gerlach TM (2007) Vapor segregation and loss in basaltic melts. *Geology* 35:
424 751–754.
425

426 Edmonds M, Gerlach TM, Herd RA (2009) Halogen degassing during ascent and eruption of
427 water-poor basaltic magma. *Chem Geol* 263: 122–130.
428

429 Edmonds M, Mather TA, Liu EJ (2018) A distinct metal fingerprint in arc volcanic emissions,
430 *Nature Geoscience* 11: 790–794. doi:10.1038/s41561-018-0214-5.
431

432 Fleet ME, Wu T-W (1993) Volatile transport of platinum-group elements in sulfide-chloride
433 assemblages at 1000°C. *Geochim Cosmochim Acta* 57: 3519–3531.
434

435 Galeczka IM, Eiriksdottir ES, Pálsson F, Oelkers E, Lutz S, Benning LG et al. (2017)
436 Pollution from the 2014–15 Bárðarbunga eruption monitored by snow cores from the
437 Vatnajökull glacier, Iceland. *J Volcanol Geotherm Res* 347: 371–396.
438

439 Gauthier P-J, Sigmarsson O, Gouhier M, Haddadi B, Moune S (2016) Elevated gas flux and
440 trace metal degassing from the 2014–15 Holuhraun eruption (Bárðarbunga volcanic system,
441 Iceland). *J. Geophys. Res. Solid Earth* 121 doi:10.1002/2015JB012111.
442

443 Gerlach TM, Graeber EJ (1985) Volatile budget of Kilauea volcano. *Nature* 313: 273–277.
444

445 Gíslason SR, Stefánsdóttir G, Pfeffer MA, Barsotti S, Jóhannsson Th, Galeczka I et al. (2015)
446 Environmental pressure from the 2014–15 eruption of Bárðarbunga volcano, Iceland.
447 *Geochem Persp Lett* 1: 84–93. doi:10.7185/geochemlet.1509.

448

449 Greenland LP, Okamura AT, Stokes JB (1988) Gases from the 1983-84 east-rift eruption. US
450 Geol Surv Pap 1463: 145-153.

451

452 Haddadi B, Sigmarsson O, Larsen G (2017) Magma storage beneath Grímsvötn volcano,
453 Iceland, constrained by clinopyroxene-melt thermobarometry and volatiles in melt inclusions
454 and groundmass glass. *J Geophys Res Sol Earth* 122. doi:10.1002/2017JB014067.

455

456 Halldórsson SA, Bali E, Hartley ME, Neave DA, Peate DW, Guðfinnsson GH et al., (2018)
457 Petrology and geochemistry of the 2014–2015 Holuhraun eruption, central Iceland:
458 compositional and mineralogical characteristics, temporal variability and magma storage.
459 *Contr Mineral Petrol* 173: 64. doi.org/10.1007/s00410-018-1487-9.

460

461 Hudson TS, White RS, Greenfield T, Ágústsdóttir Th, Brisbourne A, Green RG (2017) Deep
462 crustal melt plumbing of Bárðarbunga volcano, Iceland. *Geophys Res Lett* 44.
463 doi:10.1002/2017GL074749.

464

465 Ilyinskaya E, Schmidt A, Mather TA, Pope FD, Witham C, Baxter P et al. (2017)
466 Understanding the environmental impacts of large fissure eruptions: Aerosol and gas
467 emissions from the 2014–2015 Holuhraun eruption (Iceland). *Earth Plan Sci Lett* 472: 309–
468 322. doi.org/10.1016/j.epsl.2017.05.025.

469

470 Mather TA, Witt MLI, Pyle DM, Quayle BM, Aiuppa A, Bagnato E, et al. (2012) Halogens
471 and trace metal emissions from the on-going 2008 summit eruption of Kīlauea volcano,
472 Hawai'i. *Geochim Cosmochim Acta* 83: 292–323. doi:10.1016/j.gca.2011.11.029.

473

474 Óladóttir B, Thordarson T, Larsen G, Sigmarsson O (2007) Did the Mýrdalsjökull ice-cap
475 survive the Holocene Thermal Maximum? Evidence from sulfur contents in Katla tephra
476 layers (Iceland) from the last ~8400 years. *Ann Glaciol* 45: 183-185.

477

478 Parfitt EA., Wilson L (1994) The 1983–86 Pu' u 'O'o eruption of Kilauea volcano, Hawaii: a
479 study of dike geometry and eruption mechanisms for a long-lived eruption. *J Volcanol*
480 *Geotherm Res* 59: 179-205

481

482 Pétursson G, Pálsson PA Georgsson, G (1984) Um eituráhrif af völdum Skaftárelda (On the
483 poisoning effect of the Skaftá Fires (Laki eruption)). In: Gunnlaugsson GÁ, Gudbergsson
484 GM, Thorarinsson S, Rafnsson S, Einarsson, Th (eds) Skaftáreldar 1783-1784; ritgerðir og
485 heimildir. Mál og menning, Reykjavik, pp.81-98.

486

487 Pfeffer MA, Bergsson B, Barsotti S, Stefánsdóttir G, Galle B et al. (2018) Ground-Based
488 Measurements of the 2014–2015 Holuhraun Volcanic Cloud (Iceland). *Geosciences* 8: 29.
489 doi:10.3390/geosciences8010029

490

491 Reynolds HI, Gudmundsson MT, Högnadóttir Th, Axelsson G (2019) Changes in geothermal
492 activity at Bárðarbunga, Iceland, following the 2014–15 caldera collapse, investigated using
493 geothermal system modelling. *J. Geophys. Res. Solid Earth*. doi.org/10.1029/2018JB017290.

494

495 Sharp ZD, Barnes JD, Fischer TP, Halick M (2010) An experimental determination of
496 chlorine isotope fractionation in acid systems and applications to volcanic fumaroles.
497 *Geochim Cosmochim Acta* 74: 264–273. doi: 10.1016/j.gca.2009.09.032.

498
499 Sigmundsson F, Hooper A, Hreinsdóttir S, Vogfjörð K, Ófeigsson B, Heimisson ER et al.
500 (2015) Segmented lateral dyke growth in a rifting event at Bárðarbunga volcanic system,
501 Iceland. *Nature* 517: 191–195. doi:10.1038/nature14111.
502
503 Simmons IC, Pfeffer MA, Calder ES, Galle B, Arellano S (2017) Extended SO₂ outgassing
504 from the 2014–2015 Holuhraun lava flow field, Iceland. *Bull Volcanol* 79: 79.
505 doi.org/10.1007/s00445-017-1160-6.
506
507 Sparks RSJ (2003) Dynamics of magma degassing. In: Oppenheimer C, Pyle D, Barclay J
508 (eds.), *Volcanic degassing*. Geological Society, London, Special Publication 2213: 5-22.
509
510 Stefánsson A, Stefánsson G, Keller NS, Barsotti S, Sigurdsson Á, Thorlákssdóttir SB et al.,
511 (2017) Major impact of volcanic gases on the chemical composition of precipitation in
512 Iceland during the 2014–2015 Holuhraun eruption. *J Geophys Res Atmos* 122: 1971-1982. doi:
513 10.1002/2015JD024093.
514
515 Stelling J, Botcharnikov RE, Beermann O, Nowak M (2008) Solubility of H₂O- and chlorine-
516 bearing fluids in basaltic melt of Mount Etna at T= 1050–1250 C and P= 200 MPa. *Chem*
517 *Geol* 256: 102-110.
518
519 Swanson DA, Fabbi BP (1973) Loss of volatiles during fountaining and flowage of basaltic
520 lava at Kīlauea Volcano, Hawaii. *J Res US Geol Surv* 1: 649–658.
521
522 Swanson DA, Duffield WA, Jackson DB, Peterson DW (1979) Chronological narrative of the
523 1969–71 Mauna Ulu eruption of Kilauea volcano, Hawaii. *US Geol Surv Prof Pap* 1056: 1-55
524
525 Symonds RB, Rose WI, Bluth GJS, Gerlach TM (1994) Volcanic-gas studies: Methods,
526 results, and applications. In: Carroll MR, Holloway JR (eds) *Volatiles in magmas*. *Rev*
527 *Mineral Geochem* 30: 1–66.
528
529 Thorarinnsson S (1969) The Lakagigar eruption of 1783. *Bull Volcanol* 33: 910-927.
530
531 Thordarson T, Self S, Oskarsson N, Hulsebosch T (1996) Sulfur, chlorine, and fluorine
532 degassing and atmospheric loading by the 1783–1784 AD Laki (Skaftár Fires) eruption in
533 Iceland. *Bull Volcanol* 58: 205–225. doi:10.1007/s004450050136.
534
535 Thordarson T, Self S (2003) Atmospheric and environmental effects of the 1783–1784 Laki
536 eruption: A review and reassessment. *J Geophys Res Atmos* 108: 4011.
537 doi:10.1029/2001JD002042.
538
539 Webster JD, Kinzler RJ, Mathez A (1999) Chloride and water solubility in basalt and andesite
540 melts and implications for magmatic degassing. *Geochim Cosmochim Acta* 63: 729–738.
541
542 Zolotov MY, Matsui T (2002) Chemical models for volcanic gases on Venus. *Lun Planet Sci*
543 XXXIII, 1433.
544

545 **Table 1.** Volatile species concentrations and element mass ratios in post- (prefix HH) and syn-
 546 eruptive (prefix BARB) gas samples from the 2014-2015 Holuhraun eruption, Bárðarbunga
 547 volcanic system, Iceland. ‘Blank’ refers to the local atmosphere. Samples BARB-A and -B
 548 are taken from Gauthier et al. (2016). Residual concentration in whole-rock sample of the degassed
 549 Holuhraun lava is given as $\mu\text{g/g}$.

550
 551
 552

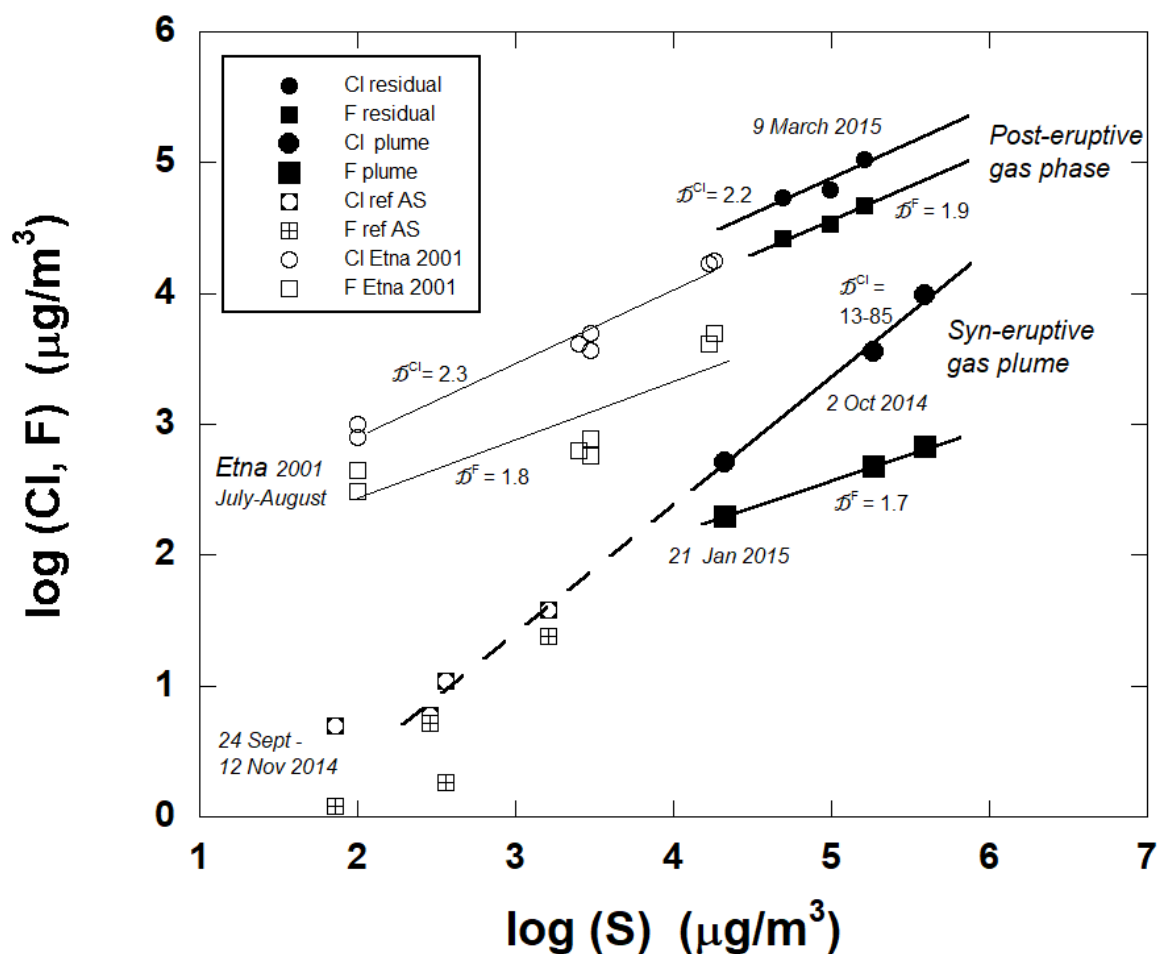
	Lava	BARB-A	BARB-B	Loc2 FP*	HH1	HH2	HH3	Blank
Sampling date	29/08/2014	02/10/2014	02/10/2014	21/01/2015	09/03/2015	09/03/2015	09/03/2015	09/03/2015
Latitude (°N)	64.85	64.87	64.87	64.89	64.85	64.85	64.85	64.86
Longitude (°W)	16.86	16.86	16.86	16.8	16.83	16.83	16.83	16.86
S (mg/m^3)	97.0	185	391	21.5	97.6	49.0	164	0.323
Cl (mg/m^3)	110	3.54	9.72	0.515	61.8	53.2	104	0.720
F (mg/m^3)	190	0.475	0.674	0.199	33.7	26.5	46.3	0.517
S/Cl mass	0.88	52	40	42	0.45	1.58	0.92	1.57
Cl/F mass	0.58	7.5	14.4	2.6	1.39	1.83	2.01	2.25
S/F mass	0.51	390	580	108	0.62	2.90	1.85	3.53
SO ₂ /HCl molar	0.97	58	44	46	1.74	1.02	1.74	0.50
HCl/HF molar	0.31	4.0	7.7	1.4	0.98	1.08	1.20	0.75
SO ₂ /HF molar	0.30	230	340	88	1.72	1.10	2.09	0.37

*airborne plume from Ilyinskaya et al. (2017)

553
 554

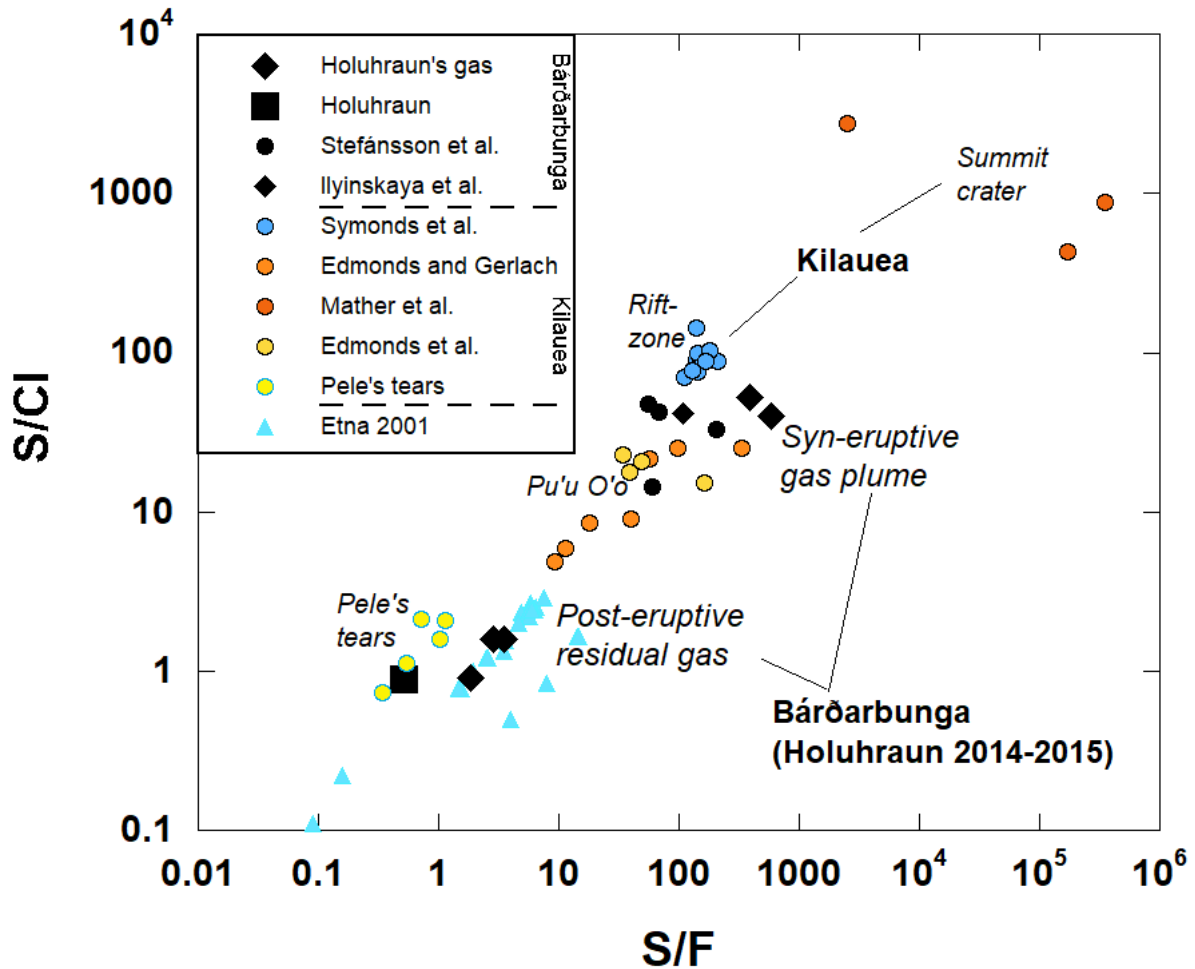


555 **Fig. 1** Grounded gas plume at Holuhraun on 2 October 2014 caused by atmospheric
 556 temperature inversion. Top left and right insets show, respectively, sampling conditions
 557 within the syn-eruptive gas plume and of the post-eruptive gas phase inside the eruptive
 558 fissure on 9 March 2015.
 559



561
 562
 563
 564
 565
 566
 567
 568
 569
 570
 571
 572
 573
 574

Fig. 2 Halogen vs sulphur concentrations in syn- and post-eruptive gas (plume and residual gas) from Holuhraun. Circles and squares denote Cl and F concentrations, respectively. The post-eruptive gas phase data are from the present study. Filled symbols for the syn-eruptive gas plume data are from Gauthier et al. (2016) and Ilyinskaya et al. (2017), whereas results from Stefánsson et al. (2017; ref AS on plot) are shown with open symbols. The squared correlation coefficient, R^2 , ranges from 0.837 for post-eruptive Cl vs S to 0.999 for syn-eruptive F vs S concentrations. Also plotted are results from Aiuppa et al. (2002) for the 2001 flank eruption on the south slope of Mt. Etna, Sicily. The vapour-melt partition coefficient ($\mathcal{D}^{V/M}$) shown is simply the reciprocal of $D^{1/g}$ calculated from the slope of the linear best-fit and by assuming $D^{1/g}$ for $S = 0$. See text for further discussion.



575
 576
 577
 578
 579
 580
 581
 582
 583
 584
 585
 586
 587
 588

Fig. 3 Mass ratios of S/Cl versus S/F illustrating the decreasing sulphur concentration from the syn-eruptive gas plume (Gauthier et al., 2016) to the post-eruptive residual gas phase at Holuhraun, Bárðarbunga volcanic system, Iceland. Also displayed are syn-eruptive results from Ilyinskaya et al. (2017) and Stefánsson et al. (2017). The Kilauea summit, rift zone and Pu'u O'o gas and Pele's tears compositions are respectively from Mather et al. (2012), Symonds et al. (1994), Edmonds and Gerlach (2006) and Edmonds et al. (2009). Kilauea rift zone and Pu'u O'o gas are of similar composition as that of Holuhraun, whereas the Pele's tears record the residual gas phase comparable to that of the post-eruptive gas and outgassed lava of Holuhraun. Gas collected during the Etna 2001 eruption displays similar exhaustion of S during fractional degassing at significantly lower S/halogens (Aiuppa et al., 2002).